Journal of Environmental Radioactivity 129 (2014) 107–120

Contents lists available at ScienceDirect

Journal of Environmental Radioactivity

journal homepage: www.elsevier.com/locate/jenvrad

Mapping the geogenic radon potential: methodology and spatial analysis for central Hungary

Katalin Zsuzsanna Szabó [a], Gyozo Jordan [b], Ákos Horváth [c], Csaba Szabó [a,*]

[a] Lithosphere Fluid Research Laboratory, Department of Petrology and Geochemistry, Eötvös University, Pázmány Péter sétány 1/C, 1117 Budapest, Hungary
[b] Institute for Geological and Geochemical Research, Research Centre for Astronomy and Earth Sciences, Hungarian Academy of Sciences, Budaörsi út 45, 1112 Budapest, Hungary
[c] Department of Atomic Physics, Eötvös University, Pázmány Péter sétány 1/A, 1117 Budapest, Hungary

ARTICLE INFO

Article history:
Received 23 August 2013
Received in revised form
2 December 2013
Accepted 12 December 2013
Available online

Keywords:
Hungarian geogenic radon potential
Soil gas radon
Soil gas permeability
Spatial modeling

ABSTRACT

A detailed geogenic radon potential (GRP) mapping based on field soil gas radon and soil gas permeability measurements was carried out in this study. A conventional continuous variable approach was used in this study for GRP determination and to test its applicability to the selected area of Hungary. Spatial pattern of soil gas radon concentration, soil permeability and GRP and the relationship between geological formations and these parameters were studied by performing detailed spatial analysis.

Exploratory data analysis revealed that higher soil gas radon activity concentration and GRP characterizes the mountains and hills than the plains. The highest values were found in the proluvial–deluvial sediments, rock debris on the downhill slopes eroded from hills. Among the Quaternary sediments, which characterize the study area, the fluvial sediment has the highest values, which are also located in the hilly areas. The lowest values were found in the plain areas covered by drift sand, fluvioeolic sand, fluvial sand and loess. As a conclusion, radon is related to the sediment cycle in the study area.

A geogenic radon risk map was created, which assists human health risk assessment and risk reduction since it indicates the potential of the source of indoor radon. The map shows that low and medium geogenic radon potential characterizes the study area in central Hungary. High risk occurs only locally. The results reveal that Quaternary sediments are inhomogeneous from a radon point of view, fluvial sediment has medium GRP, whereas the other rock formations such as drift sand, fluioeolic sand, fluvial sand and loess, found in the study area, have low GRP.

1. Introduction

The adverse health effects of radon are well documented (e.g. WHO, 2009). Regulation and mitigation is therefore envisaged which among other measures requires knowing the geographical extent of the hazard related to radon. The radon risk is often defined as the probability that indoor radon exceeds a risk; the geogenic source of the hazard (or potential risk) at a location or over an area is described by its radon potential.

Knowledge on the radon potential of an area can support decisions on whether further local measurements are necessary in the areas of planned development. Factors influencing indoor radon concentration are living habits such as ventilation and building structure, including building material or presence and type of basement and cellar below the house. The geogenic radon potential (GRP) shows the potential of the source of indoor radon 'what the Earth delivers' because generally the subsurface (soil gas radon concentration) is the main source for indoor radon concentration (UNSCEAR, 2000). The GRP is independent from the influence of any building related or living habit factors. Besides this, the relationship between soil gas radon concentration and indoor radon concentration is well known (Appleton and Miles, 2010; Barnet et al., 2005; Barnet, 2011; Barnet and Pacherová, 2010; Chen et al., 2009; Kemski et al., 2005).

In 2008 the Radioactivity Environmental Monitoring (REM) group at the Institute for Transuranium Elements (ITU), Joint Research Centre (JRC) decided to compile a geogenic radon map of Europe in the frame of preparing a European Natural Radiation Atlas (De Cort, 2010). In contrast to the indoor radon map of Europe that covers only areas where indoor measurements are available, the geogenic map will present the radon potential at any location in Europe using geological, soil data and soil gas radon measurements (De Cort, 2010). However, several definitions of a quantity "radon

* Corresponding author. Tel.: +36 1 372 2500x8338; fax: +36 1 361 2212.
E-mail addresses: sz_k_zs@yahoo.de (K.Z. Szabó), gyozojordan@gmail.com (G. Jordan), akos@ludens.elte.hu (Á. Horváth), cszabo@elte.hu, cszaboo@yahoo.com (C. Szabó).

0265-931X/$ – see front matter © 2013 Elsevier Ltd. All rights reserved.
http://dx.doi.org/10.1016/j.jenvrad.2013.12.009

potential" exist in the literature (Alonso et al., 2010; Barnet et al., 2005; Barnet and Fojtíková, 2008; Barnet and Pacherová, 2010; Chen, 2009; Chen et al., 2012; Neznal et al., 2004; Dehandschutter and Ciotolli, 2010; Friedmann, 2005; Guida et al., 2010; Ielsch et al., 2010; Kemski et al., 2001; Miles et al., 1991; Miles and Appleton, 2005; Tóth et al., 2006; Schumann, 1993), which sometimes causes confusion. One suggested approach to quantify the geogenic radon potential for the geogenic radon map of Europe is the continuous variable (formerly radon index) developed by Neznal et al. (2004) (Eq. (1)):

$$\mathrm{GRP} = \frac{c_\infty}{-\log_{10} k - 10} \quad (1)$$

where c_∞ is the equilibrium soil gas radon activity concentration at a definite depth (0.8–1 m) (kBq m^{-3}) and k is the soil gas permeability (m^2). Based on many years of extensive research in the Czech Republic, three categories of GRP (Eq. (1)) were set: low (GRP < 10), medium (10 < GRP < 35) and high (35 < GRP) (Neznal et al., 2004). The geogenic radon potential of Neznal et al. (2004) is based on the radon index classification table formerly used in the Czech Republic (Barnet, 1994).

In many cases soil gas radon concentration is subject to temporal variation and the seasonal variation is mostly higher than the diurnal one (Al-Shereideh et al., 2006; Barbosa et al., 2007; Baykut et al., 2010; Crockett et al., 2010; Dubois, 2005; Neznal et al., 1995; Neznal and Pernička, 1996; Neznal and Neznal, 2006; Perrier et al., 2009; Smetanová et al., 2010; Sundal et al., 2008; Szabó et al., 2013; Winkler et al., 2001). Seasonal variation of soil gas radon concentration can have great impact on the value of c_∞ in case of a single local point measurement, and therefore on its representativeness for the location.

In Hungary, several indoor radon surveys were performed in the last decades and indoor radon potential maps have been made (Hámori et al., 2006a,b). Strong dependence of indoor radon measured at one-storied houses with no basement on the geological background was demonstrated (Minda et al., 2009). Soil gas radon measurements were also performed by several institutes and universities for research purposes, such as during the rehabilitation processes in the area of the closed uranium mine (Mecsek Mts, SW-Hungary) (Somlai et al., 2006). However, geogenic radon potential mapping has not been performed in Hungary yet.

The main aim of this study is to present a detailed GRP mapping based on soil gas radon and soil gas permeability measurements and to create a radon risk map that helps regional planning. In this study, the continuous variable approach (Eq. (1)) was used for GRP determination. A further objective is to characterize geological formations with radon, soil gas permeability and geogenic radon potential based on field measurement results. In addition, a detailed spatial analysis using local trend analysis, variogram and autocorrelation analysis and regression analysis were carried out to reveal and numerically describe spatial patterns in the three parameters (radon concentration, soil gas permeability and geogenic radon potential). The specific objective was to develop a GRP map for the studied region including Hungary's capital city Budapest and surrounding area, in order to assist human health risk assessment and risk reduction.

2. Study area

The study area is located in the Pannonian Basin and includes Budapest, the majority of Pest County (PC), the westernmost part of Nógrád County (NC) and some areas from other adjacent counties (Komárom-Esztregom County: KC, Fejér County: FC) (Fig. 1). The 80 × 90 km highest extension of study area encompasses 5400 km^2 covering 6.5% of the country. This part of Hungary has the highest

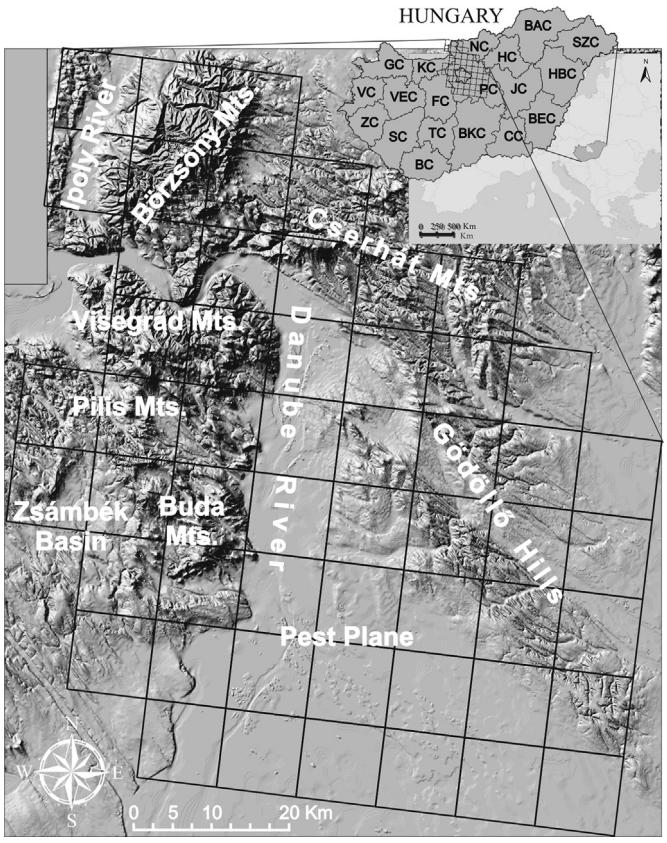

Fig. 1. Shaded relief map of the study area showing joining point of the two highest Hungarian mountain ranges, the North Hungarian Mountains and the Transdanubian Mountains with the Great Hungarian Plane on either side of River Danube. Inset: location of the studied Pest County and some of the neighboring counties. FC – Fejér County, KC – Komárom-Esztergom County, NC – Nógrád County, PC – Pest County.

population density: 28% (2.83 million) of the population of the country (9.9 million) live in the 220 settlements of the study area. The area is also characterized by diverse geological background, thus providing excellent conditions for radon risk mapping and geological modeling research.

The diverse geological background can be related to the joining point of the two highest Hungarian mountain ranges, the North Hungarian Mountains and the Transdanubian Mountains with the Great Hungarian Plane. Accordingly, there are hills (the highest elevation is 938 m asl.) along the longitudinal extension (N–S direction) in the western part of the area. The Danube River enters the study area from west and sharply turns to the south at the Danube Bend, an intense touristic area. The Northeast part is hilly (Cserhát Mts. and Gödöllő Hills with the highest elevation 652 and 345 m asl., respectively). Northwestern part of the Great Hungarian Plane, the Pest plane covers the middle and southern parts (100–150 m asl.) of the study area (Fig. 1).

The northernmost part of the study area comprises the Miocene volcanic andesite and dacite areas of the Visegrád Mts. and Börzsöny Mts. over the Tertiary sedimentary basin covering the Paleozoic crystalline basement. Along the Ipoly River, a Holocene alluvial plain (mud and sand) is found. On the Mesozoic carbonates formation Eocene and Oligocene limestone, marl and sandstone evolved in the Pilis Mts., whereas Triassic limestone, dolomite and marl build up the Budai Mts. In the foreground of the Budai Mts. lays the Zsámbék Basin. It consists of Pliocene clay, sand, gravel in the western part, Miocene clay and limestone in the middle and eastern part and Pleistocene loess in the southern part. The Mesozoic and Paleozoic strata of the Pest Plane and Gödöllő Hills is covered by several

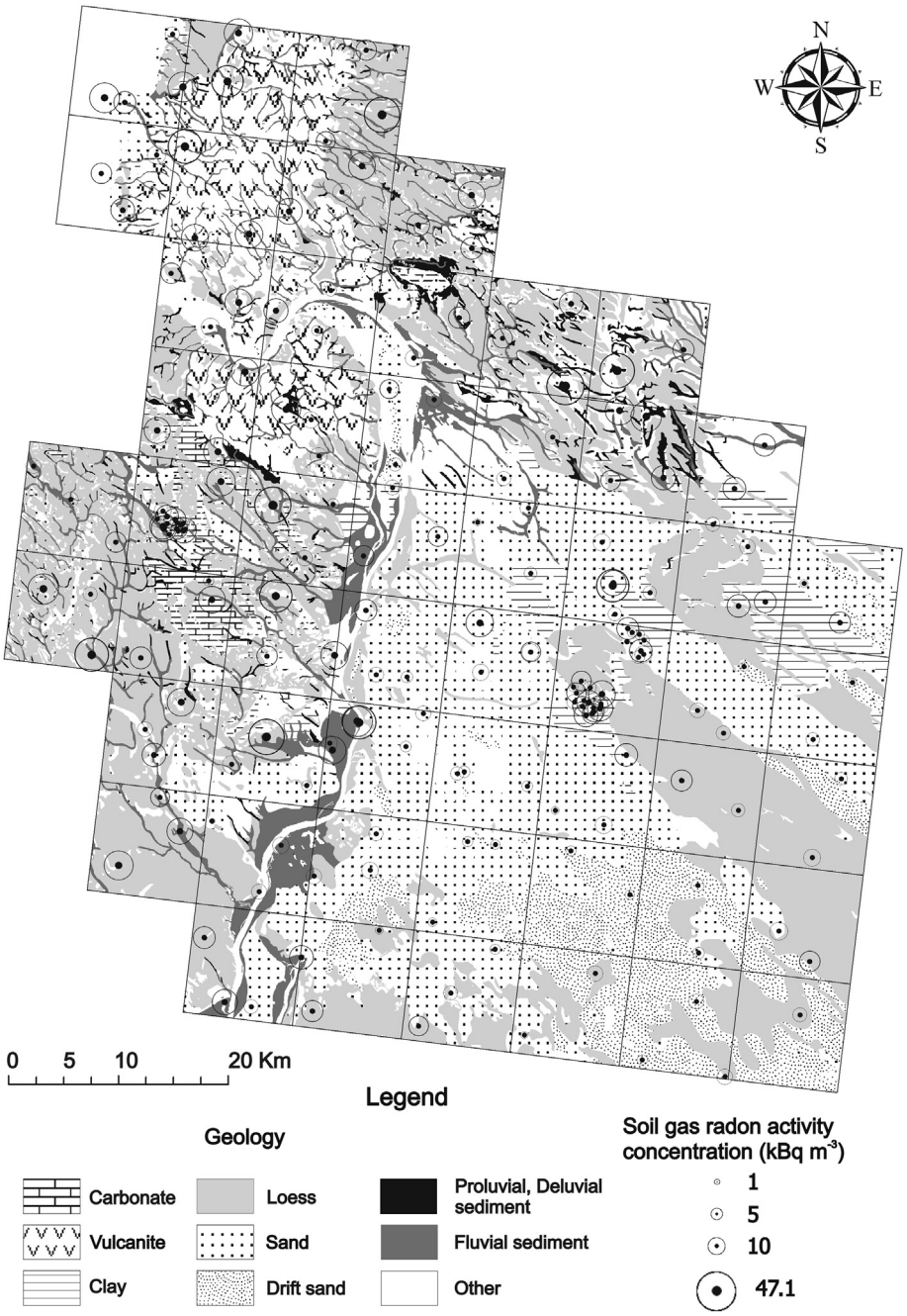

Fig. 2. Simplified geology of the study area with the measurement sites (solid dots). Radius of the empty circles of the post map corresponds to soil gas radon activity concentration (kBq m^{-3}) values.

hundred meters Holocene, Pleistocene, Pliocene and Miocene sediments such as sand, drift sand, gravel, loess, marl, silt, clay or limestone (Gyalog, 1996). The geological units in the hilly areas are meshed with recent or paleo-rivers providing Quaternary fluvial sediment in the valleys of the mountains. Geological formations of the study area give almost the whole diversity of Hungarian geology, except the Paleozoic sediments, granite and crystalline rocks (Gyalog, 1996; Minda et al., 2009) (Fig. 2).

Hungary has temperate continental climate with a long-term annual average temperature of 11 °C with warm summers (20 °C), cold winters (0 °C) and mild springs and autumns (10 °C). The annual average precipitation is 500–550 mm. The precipitation falls mostly during the summer months (especially June) and the least in the winter season (especially February) based on the Hungarian Meteorological Service (OMSZ) database (www.met.hu/eghajlat/magyarorszag_eghajlata).

3. Materials and methods

3.1. Field measurement

Soil gas radon activity concentration was measured in situ with a RAD7 Electronic Radon Detector (Durridge Company Inc., 2000) coupled with soil probe through a small drying tube. The inner diameter of the soil probe is ¼ inch. The soil gas was pumped out from (if possible) generally 0.8 m depth of the soil. The soil probe was hammered to 85 cm and pulled back for 5 cm. The instrument setting was “Grab” protocol (Durridge Company Inc., 2000). It initiates a

standard grab sampling sequence at the beginning of a run. At the beginning the pump runs for exactly 5 min. This is followed by a 5-min. equilibrium delay to reach equilibrium between ^{222}Rn and ^{218}Po, after which the counting period begins. The pump does not operate during the counting period which is four 5-min count cycles. The total time of the measurement is therefore 30 min. Soil gas radon activity concentration was determined by averaging the results of the four 5-min counting periods. In "Sniff Mode" the device calculates the radon activity concentration from the 3-min half-life ^{218}Po alpha peak at 6.0 MeV and gives radon activity concentration in Bq m^{-3} unit. The rate of flow of the pump is 1 L min^{-1}. The RAD7 was calibrated in 2009 and the calibration is highly stable according to the manufacturer specifications (Durridge Company Inc., 2000). Typical drift is less than 2% per year. The uncertainty (two-sigma) of RAD7 with a 5-min counting cycle is about 40%, 10%, 8% and 5% in case of 1, 10, 20, 40 kBq m^{-3} radon activity concentration values, respectively. According to the comparison measurements with the RAD7 detector of the Hungarian "Frédéric Joliot-Curie" National Research Institute for Radiobiology and Radiohygiene and the LUK3C scintillation detector of the Babes-Bolyai University, Cluj (Romania) calibrated in 2010, we found that the detectors measure the same radon concentration at a 95% confidence level.

Soil gas permeability measurement was performed immediately after the soil gas radon measurement by Radon-JOK equipment (Radon v.o.s.) coupled with the same soil probe. Calculation of the gas permeability was based on Darcy's equation (Koorevaar et al., 1983) according to the equipment manual (Radon v.o.s.). The equipment works with air withdrawal by means of negative pressure. Air is pumped from the soil under constant pressure through the probe with a constant surface of contact between the probe head and the soil. The constant active area is created at the end of the probe (driven into the soil to the measurement depth) by pulling the probe back by 5 cm. The special rubber sack with one weight pumps the air from the soil and allows performing measurements at very low pressures. The gas permeability (k) is calculated from Eq. (2) using the measured air flow through the probe. The air flow is defined by the known air volume in the rubber sack and by the measured pumping (sinking) time. The soil is assumed to be homogeneous and isotropic and a standard state is considered. Furthermore, the air is assumed to be incompressible (pressure differences are very much smaller than atmospheric pressure). The air flow can be expressed by the following equation:

$$Q = \frac{Fk\Delta p}{\mu} \tag{2}$$

where Q is the air flow through the probe (m^3 s^{-1}), F is the shape factor of the probe (m), k is the gas permeability of the soil (m^2), Δp is the pressure difference between surface and the active area of the probe (Pa), μ is the dynamic viscosity of air (Pa s).

The shape factor, F, was calculated after Damkjaer and Korsbech (1992) and van der Graaf and de Meijer (1992):

$$F = \frac{2\pi L}{\ln\left(\frac{2L}{d}\sqrt{\left(\frac{4D-L}{4D+L}\right)}\right)} \tag{3}$$

where L is the length of the active area of the probe head (m), D is the depth below the surface (m), d is the diameter of the active area (m). The air flow, Q, is calculated using Eq. (4):

$$Q = Av \tag{4}$$

where A is the surface of the flow volume (m^2), v is the velocity of the air (m s^{-1}). During the gas permeability measurement, the sinking time on a known distance was measured, from which v (Eq. (4)) can be calculated. The Radon-JOK permeameter has it's own ~1 s sinking time, which is neglected in the calculation of v (Eq. (4)) according to the equipment manual (Radon v.o.s.). During soil gas permeability measurements a thinner RAD7 pipe was used. The inner diameter of the pipe was 33% thinner (0.6 mm) than the original one (0.9 mm), hence the permeameter has a non negligible sinking time (an additional 7.3 s) that we subtracted from the measured sinking time value. There was only one site having higher than 1E−10 m^2 permeability due to measurement uncertainty. This site was excluded from further analysis of permeability since GRP cannot be calculated from this value.

The bases of the site selection were the extension of geological formations and the distribution of settlements (built-up areas). The internationally suggested 10 × 10 km grid for the European indoor radon map (Dubois et al., 2010; Tollefsen et al., 2011) helped to achieve a spatially uniform sampling. On average, three measurement sites were taken in each cell, which results in 3.2 km average nearest-neighbor distance between the 192 measurement sites. The three dominating geological formations were selected in the cell and a measurement in each formation was made, also taking the locality of the towns into account. We preferred geological formations inside and around the settlements since these are the target areas for planned building developments. In case of two settlements, the sampling distance was reduced below 1 km. Thus, the sampling scheme is similar to a stratified (grid-based) random sampling. At each site, one "Grab" soil gas radon and one soil gas permeability measurement was made.

Measurements were performed in all months (i.e., from May 2010 to December 2011), but mostly in summer, from May to September (85% of the measurements), to reduce the possible effect of the seasonality. Measurements were performed between 7:30 am and 9:00 pm.

In many cases air temperature, humidity and the absolute pressure by a Touch Screen Weather Station PCE-FWS 20 (PCE Instruments UK Ltd.) were also measured. Geographic coordinates for the 192 measurement sites were determined by GPS.

3.2. Database

The obtained data set consists of the measurement ID, the sampling site coordinates, the measurement date and time, the depth of measurement, the measured four 5-min soil gas radon activity concentration values, the measured sinking time data (for soil gas permeability), and air temperature, humidity and absolute pressure. Additional computed data are also in the database such as the soil gas radon activity concentration calculated by averaging the results of the four 5-min. counting periods. Soil gas permeability was calculated from Eq. (2) and geogenic radon potential was calculated using Eq. (1). Geological information (i.e., rock type, age and fault lines) was taken from the 1:100,000 digital Geological Map of Hungary (Gyalog and Síkhegyi, 2010).

3.3. Statistical analysis

Summary statistics used in this study include measures of central tendency and variability. These statistics are the minimum, lower quartile, median, upper quartile, maximum and average (arithmetic mean), mode, standard deviation, median absolute deviation (MAD), range and inter-quartile range. Tukey's (1977) inner-fence criteria were used for outlier definition and the robust MAD/median measure is used for comparison of variability of parameters. Spatial radon measurements empirical distribution often has heavy-tail property and in many cases outliers indicate real anomalies. This was confirmed by several authors (Appleton

et al., 2011; Bertolo and Verdi, 2001; Bossew et al., 2008; Kemski et al., 2001; Tóth et al., 2006).

The Kruskal–Wallis and Mann–Whitney Tests (Kruskal and Wallis, 1952; Mann and Whitney, 1947) were applied under the null hypothesis that the medians of measured parameters (soil gas radon activity concentration, soil gas permeability, GRP) within each of the geological formations are the same. Levene's Test (Levene, 1960) was applied to test the null hypothesis if the standard deviations within each of the geological formations are the same. Kolmogorov–Smirnov Test (Kolmogorov, 1933; Smirnov, 1948) was applied to test the null hypothesis if the distributions of two datasets are homogeneous.

Simple least-squares linear regression analysis with constant additive was performed to explore the linear relationship between the meteorological parameters (atmospheric temperature, humidity and absolute pressure) and soil gas radon concentration, soil permeability and geogenic radon potential. Strength of relationship is expressed by the Pearson's linear correlation coefficient (r) (Rodgers and Nicewander, 1988). All of the statistical tests applied in this study were at 95% confidence level.

3.4. Mapping and spatial analysis

Field-measured soil gas radon activity concentration, soil gas permeability and calculated geogenic radon potential were plotted on post maps to observe their spatial distribution and possible association with geological formations. On the post map circles indicate the measurement sites and the radius of the circle is linear proportional to the quantity of the value.

In order to study the large-scale spatial trend in the measured parameters a smoothing procedure was applied to filter the small-scale 'noise' from the data. This spatial characterization is based on contour map generated with the linear and accurate (fitting to the original measured values at sample locations) Triangular Irregular Network (TIN) interpolation (Guibas and Stolfi, 1985). Grid size of 250 m was used based on the shortest distance between the closest two measurement sites. Successive moving average smoothing was applied to generalize the TIN model and to capture the major spatial trends of radon and other parameter distribution. First, a series of 3×3, 9×9, 13×13, 17×17, 21×21 and 31×31 window size moving average low-pass filter smoothing was applied to the original 250 m spaced TIN maps. The 21×21 (5250×5250 m) window size smoothed TIN maps revealed the spatial trends and pattern without losing much detail and they were used for spatial autocorrelation and directional variogram calculations.

Spatial radon risk assessment used the median, upper quartile and internationally defined GRP limits (Neznal et al., 2004) to identify areas of interest. Directional empirical variograms were calculated to capture and quantitatively describe spatial anisotropy and periodicity. In addition to the variogram analysis, 2D autocorrelograms were made also to reveal anisotropy and periodicity present in the spatial data.

The conventional approach of European geogenic radon mapping for visualization of the geogenic radon potential in a map is providing a GRP value for each geological formation. Thus, a GRP risk map was compiled from median GRP values calculated for the geological formations based on the field measurements. Spatial modeling was performed with Surfer and ArcGIS applications.

4. Results

4.1. Statistical analysis

Each of the measured parameters were found unimodal and internally homogeneous, apart from the occasional outliers, according to the method of Reimann et al. (2008). Summary statistics of soil gas radon activity concentration, soil gas permeability and GRP of the 192 sites are shown in Table 1. Soil gas radon activity concentration data have a minimum 1 kBq m^{-3}, a maximum 47 kBq m^{-3}, a median 10.9 kBq m^{-3} and an average 14.1 kBq m^{-3} with a standard deviation 10.2 kBq m^{-3} (Table 1). Ten high outliers existed in data: higher than 35.9 kBq m^{-3}. One of these outliers is in Tertiary clay but all the others are in Quaternary sediments, such as proluvial–deluvial sediment, fluvial sediment, sandy loess and loess. According to the Kolmogorov–Smirnov and the Chi-square tests, soil gas radon concentration data can be described by lognormal distribution at the 95% confidence level. Soil gas permeability has a minimum 9.8E−14 m^2, a maximum 6.6E−11 m^2, a median 4.4E−12 m^2 and an average 9.6E−12 m^2 with a standard deviation 1.3E−11 m^2 (Table 1). Twenty-three high outliers existed in the soil gas permeability data: higher than 2.4E−11. According to the Kolmogorov–Smirnov and the Chi-square tests, the data conformed to lognormal distributions. Geogenic radon potential data have a minimum 0.9, a maximum 74.2, a median 8.1 and an average 12.0 with a standard deviation 11.4 (Table 1). Twenty-three high outliers had values higher than 22.7. According to the Kolmogorov–Smirnov and the Chi-square tests, the data conformed to lognormal distributions.

The 192 measurement sites belong to 41 different geological formations based on the 1:100,000 digital Geological Map of Hungary. The Kruskal–Wallis test showed a statistically significant difference amongst the medians of the soil gas radon activity concentration in the 41 geological formations at the 95% confidence level ($p = 0.001$). The Levene's test indicated no statistically significant difference amongst the standard deviations at the 95% confidence level ($p = 0.08$). Values of soil gas radon concentrations measured on different geological formations were plotted in a box and whiskers diagram (Fig. 3). Since 36 out of the 41 formations had less than 9 samples, statistically reliable information can be derived only from the 5 geological formations containing more than 8 sample points, which is a criterion for the Mann–Whitney homogeneity test. The median of soil gas radon activity concentrations of these formations in increasing order are drift sand (3.6 kBq m^{-3}), fluvioeolic sand (8.0 kBq m^{-3}), fluvial sand (8.3 kBq m^{-3}), loess (13.9 kBq m^{-3}) and fluvial sediment (21.9 kBq m^{-3}). This confirms an assumption that Quaternary sediments are inhomogeneous for radon emanation (Fig. 3, Table 2). Fluvial sediments, covering the valleys of mountains, have the highest soil gas radon activity concentration values. The other four types of Quaternary sediments can be found in the plains.

Similarly, medians of GRP values of the 41 geological formations were statistically significantly different, but their standard

Table 1
Summary statistics of soil gas radon activity concentration (kBq m^{-3}) soil gas permeability (m^2) and GRP data of the 192 sites.

Summary statistics	Count	Minimum	Lower quartile	Median	Upper quartile	Maximum	Average	Standard deviation	MAD	Range
Soil gas radon activity concentration (kBq m^{-3})	192	1.0	6.8	10.9	19.1	47.1	14.1	10.2	5.7	46.2
Soil air permeability (m^2)	191	9.8E−14	9.0E−13	4.4E−12	1.3E−11	6.6E−11	9.6E−12	1.3E−11	3.9E−12	6.6E−11
GRP	191	0.9	4.9	8.1	14.8	74.2	12	11.4	4	73.3

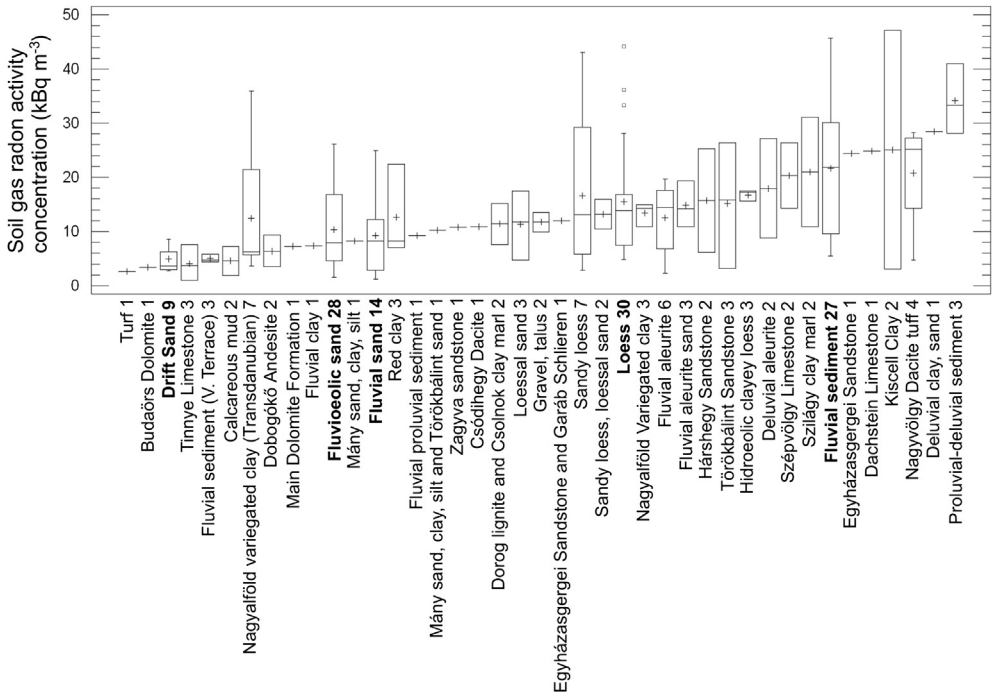

Fig. 3. Box and whisker diagram of the soil gas radon activity concentration on different geological formations, available in the study area, in increasing order of the median. Figures show the number of measurements sites at each geological formation. Bold indicates geological formations with more than 8 samples considered as dominant rocks in this paper.

deviations were not significantly different from each other according to the Kruskal–Wallis ($p < 0.05$) and Levene's ($p = 0.26$) tests, respectively. Plotting the box and whisker plots of GRP values of different geological formations, in the increasing order of medians, follows the order of low (GRP < 10), medium (10 < GRP < 35) and high GRP (35 < GRP) categorization (Fig. 4). There are 26 formations in the low, 12 formations in the medium and 2 formations in the high GRP category (Fig. 4). The two high GRP geological formations are based on one measurement of each (GRP = 45 and 51 with ~15% uncertainty), and we assume that these values uniformly characterize these two formations. The median of GRP values of the $n > 8$ geological formations are almost in the same order as in the case of the soil gas radon activity concentration (Table 2). The use of the GRP values, which consider the soil gas permeability in contrast to the original radon concentrations, had an effect on the radon risk ranking of the fluvial sand and the fluvioeolic formations.

Medians and standard deviations of soil gas permeability values of the 41 geological formations were not statistically significantly different from each other according to the Kruskal–Wallis Test ($p = 0.14$) and Levene's Test ($p = 0.6$). If we arrange the medians of soil gas permeability of different geological formations in ascending order, a monotonic increase can be observed, where break-points cannot be recognized. Therefore, there are no obvious separable groups. Considering only the 5 formations having more than 8 samples, loess has the lowest and drift sand has the highest soil gas permeability (Fig. 5).

Comparing the average permeability values of the five Quaternary sediments ($n > 8$) to the average soil gas radon activity concentrations, a high negative linear correlation ($r = -0.92$) was revealed, except for the fluvial sediment (Fig. 5). Fluvial sediment had the highest soil gas radon concentration among the 5 Quaternary formations in spite of its high soil gas permeability (Fig. 5).

4.2. Regression analysis: relationship between the measured parameters

Simple bivariate regression analysis between meteorological parameters and soil gas radon activity concentration, soil gas

Table 2
Summary statistics of soil gas radon activity concentration (kBq m^{-3}) and GRP data of the $n > 8$ geological formations.

		Count	Minimum	Lower quartile	Median	Upper quartile	Maximum	Average	Standard deviation	MAD	Range
Drift sand	Soil gas radon activity concentration GRP	9	2.7	2.9	3.6	6.3	8.6	4.9	2.3	0.9	5.9
			2.6	4.1	4.7	5.7	7.0	4.8	1.5	1.0	4.3
Fluvioeolic sand	Soil gas radon activity concentration GRP	28	1.6	4.6	8.0	16.8	26.1	10.3	6.8	4.3	24.5
			1.2	4.6	7.4	12.6	22.0	8.9	5.6	3.9	20.8
Fluvial sand	Soil gas radon activity concentration GRP	14	1.2	2.9	8.3	12.2	24.9	9.2	7.0	4.6	23.8
			0.9	3.1	5.1	7.7	20.8	6.7	5.5	2.5	19.9
Loess	Soil gas radon activity concentration GRP	30	4.9	7.5	13.9	16.8	44.1	15.5	9.7	6.1	39.2
			1.4	6.1	9.4	12.7	56.7	12.4	11.7	3.3	55.3
Fluvial sediment	Soil gas radon activity concentration GRP	27	5.5	14.5	21.9	30.1	45.7	22.2	11.1	7.8	40.2
			4.8	9.1	18.3	25.0	74.2	20.7	15.7	8.6	69.3

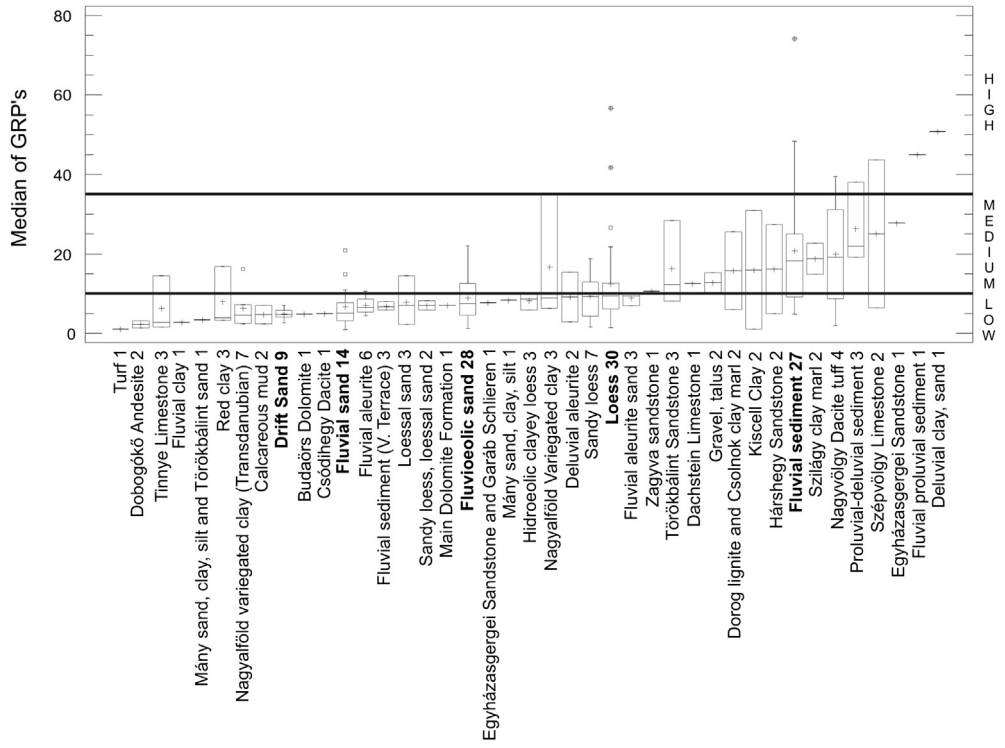

Fig. 4. Box and whisker diagram of the GRP on different geological formations in increasing order of the median. Figures show the number of measurements sites at each geological formation available in the study area. Bold face indicates geological formations with more than higher than 8 sample numbers considered as dominated rocks in this paper. Borders of GRP categories are indicated with horizontal solid lines as high, medium and low mean GRP categories according to Kemski et al. (2001).

permeability and GRP showed no significant linear relationships. All correlation coefficients were below 0.17. However, it is clear from the scatter plots (not shown) that above 30 °C air temperature the soil gas radon concentration values were always lower than 20 kBq m^{-3}. Since 30 °C can occur in the daytime in temperate continental climate, this is readily explained by the fact that formation of the convective boundary layer in the daytime, due to the insolation and consequential ground surface heating caused depletion of soil gas radon concentration (Kumar et al., 1999; Szabó et al., 2013).

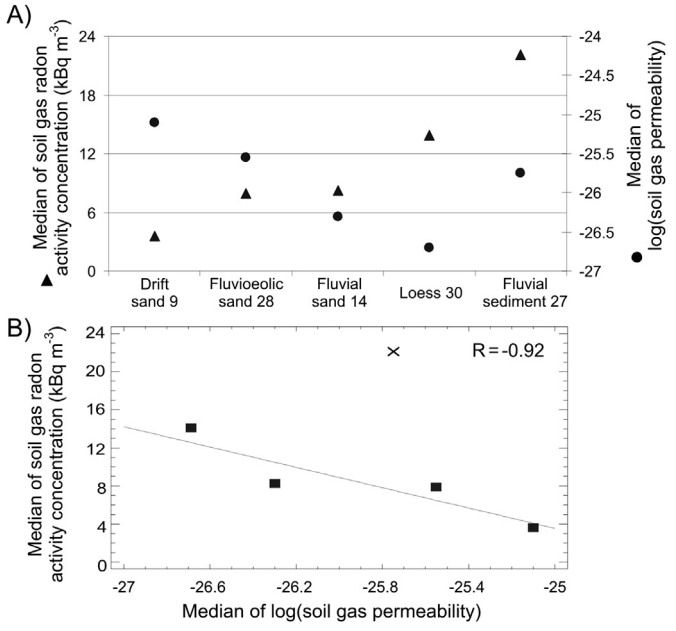

Fig. 5. A. Medians of soil gas radon activity concentration (solid triangle) and soil gas permeability (solid dot) on 5 formations having higher than 8 sample sites, arranged in increasing order of soil gas radon activity concentration. B. Negative linear correlation between median soil gas radon activity concentration and soil gas permeability. Cross symbols indicate the outlier corresponding to the fluvial sediment. *R* indicates the correlation coefficient without the fluvial sediment. Soil gas permeability values are in logarithmic scale.

We studied the relationship between the soil gas radon activity concentration, soil gas permeability and GRP, too. The GRP was lower than 35 below soil permeability 8.4E−12 m^2. Thus, all of the 12 high GRP values had permeabilities above 8.4E−12 m^2, which is considered as high permeability. When the GRP is plotted versus soil gas radon activity concentration (Fig. 6), the average soil gas permeability can be determined from the equation of the regression line ($r = 0.8$). The average soil gas permeability after outlier rejection (21 data points) was 1E−12, which corresponds to a medium value. All of the 21 outliers were above the regression line (Fig. 6), which indicates that at these 21 sites the very high soil gas permeability itself caused high GRP despite of low soil gas radon activity concentration value. Five outliers belong to the <10 kBq m^{-3} soil gas radon activity concentration category, the others correspond to the >10 kBq m^{-3} soil gas radon activity concentration category.

4.3. Mapping and spatial analysis

The smallest grid cell that resolves all measurement points for the interpolated parameter surfaces is defined by the two closest points located 9.5 m apart from each other found in one garden. This would imply an unmanageable high grid density in the 80 × 90 km study area. Based on a trial-and-error approach, a 250 m grid size proved to be the optimal compromise between the loss of information (8 data pairs fall in shared grid cells, 4.2% of all data) and digital data processing efficiency. The original 250 m spaced TIN map and the 21 × 21 (5250 × 5250 m) window size

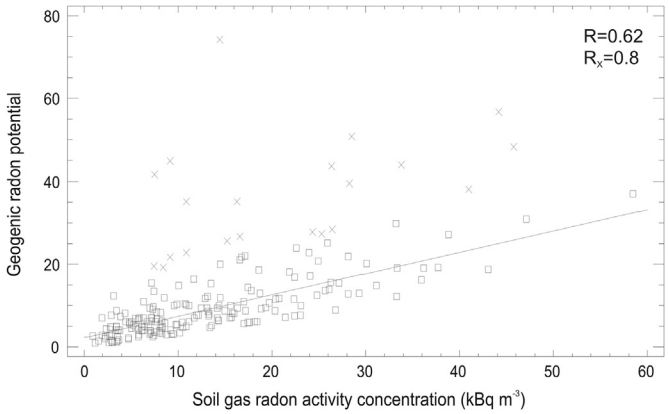

Fig. 6. Results of the simple bivariate regression analysis between geogenic radon potential and soil gas radon activity concentration. R is the correlation coefficient for all the data. R_X shows the correlation coefficient without the outliers indicated with crosses.

moving average low-pass filter smoothed map of the soil gas radon activity concentration, soil gas permeability and geogenic radon potential are shown in Fig. 7.

The soil gas radon activity concentration map has a spatial pattern according to the post map and the contour map generated from the 21 × 21 (5250 × 5250 m) window size smoothed TIN trend surface map (Figs. 2, 7 and 8). Higher values (30 kBq m^{-3} on average) are in the hilly areas in the Buda Mts., Pilis Mts., Visegrád Mts. and in the northern areas in the Börzsöny Mts. and Cserhát Mts. Lower values (9.5 kBq m^{-3} on average) characterize the southern and eastern plane areas such as the Pest Plane (Figs. 1, 7 and 8). The empirical variogram of the original soil gas radon activity concentration data without outliers has high nugget effect (Fig. 9) showing that, besides the presence of measurement error, this parameter has high variability at distances smaller than the sampling interval (according to the nearest-neighbor distance, the average sampling interval is 3.2 km).

Soil gas permeability has often highly skewed distribution, like in our case, and the extreme values have a significant impact on the variogram. Thus, the data were log-transformed prior to analysis. The log-transformed soil gas permeability data had a bimodal characteristic, however, it had no obvious spatial pattern (Fig. 7). The empirical variogram of the original soil gas permeability data without the outliers had a very high level nugget effect (Fig. 9) confirming that this parameter has a very high variability already at distances smaller than the sampling interval (3.2 km).

The calculated GRP spatial pattern was less variable than the soil gas radon concentration according to the post map and smoothed TIN trend surface map (Fig. 7). However, GRP displays the same spatial pattern: high values (median ≥ 22) are in the hilly areas and low values (median ≤ 9) characterize the southern and eastern plain areas (Figs. 1 and 7). The empirical variogram of the original GRP data without the outliers had a lower nugget effect than soil gas radon activity concentration.

5. Discussion

Between soil gas radon activity concentration and soil gas permeability, except for the fluvial sediment, a negative linear correlation was observed (Fig. 5b). Thus, soil gas radon concentration was highly variable on fluvial sediment, thus it is less predictable than for the other Quaternary sediments. Additionally, in spite of the high soil gas permeability of the fluvial sediment, it had the highest soil gas radon concentration among the 5 Quaternary

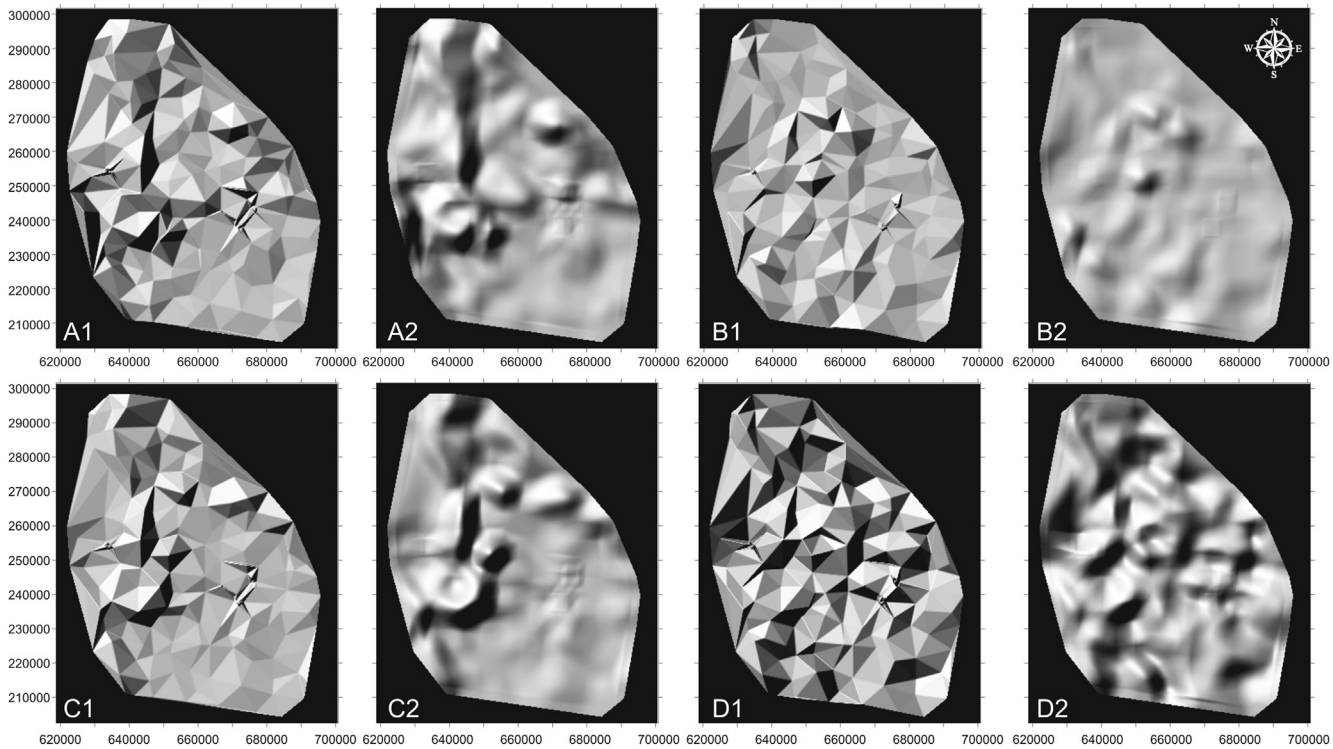

Fig. 7. Results of the smoothing procedure on the TIN maps of soil gas radon activity concentration (A), soil gas permeability (B) (also in logarithmic scale (D)) and geogenic radon potential (C). First maps (A1, B1, C1 and D1) are TIN maps made from original data. Second maps (A2, B2, C2 and D2) are the 21 × 21 (5250 × 5250 m) window size smoothed TIN maps, which revealed the spatial trends and pattern without losing much detail. They were used for spatial autocorrelation and directional variogram calculations. Coordinates are in meters.

formations with more than 8 samples. Soil gas radon activity concentration in the mountains had a median 28.1 kBq m^{-3} based on 36 values. Note that two sites were excluded because they were on artificial land filling. They correspond to the average concentrations of these types of geological formations (Kemski et al., 2001). In the area of the Tertiary andesitic and dacitic volcanic rocks of the Visegrád Mts. and Börzsöny Mts., soil gas radon activity concentrations had a median of 27.3 kBq m^{-3}, in the area of Triassic limestone and dolomite concentration values had a median of 27.1 kBq m^{-3}, and the area of Tertiary sandstone, marl and clay the median was 30.2 kBq m^{-3} based on 10, 7 and 16 data.

Additionally, these mountainous areas are nested in the valleys with Quaternary fluvial sediment, which had the highest soil gas radon activity concentration among the Quaternary sediments. In contrast, local basins covering the 80% of the study area were characterized by lower soil gas radon concentrations: 156 measurements had a median of 8.6 kBq m^{-3} value. These local basins are covered with Quaternary sands (i.e., drift sand, fluvioeolic sand, fluvial sand) and loess, which have generally low soil gas radon concentrations, as Kemski et al. (2001) and Barnet (2008) pointed out studying Cenozoic, Mesozoic and Paleozoic sedimentary rocks in Germany and magmatic, volcanic, metamorphic and sedimentary rocks in the Czech Republic, respectively.

In summary, elevated radon seemed to be related to the erosion phase of the sediment genesis. The easily eroding minerals, such as feldspar or mica and other silicates and carbonates, are deposited near to the sources in the mountains and hills as proluvial and deluvial sediments much reflecting the original rock composition such as andesite, dacite and limestone (Pettijohn, 1975). The rest of the eroded material is transported far and deposited on the plains as mature sediment composed of resistant minerals such as dominating quartz and minor zircon, apatite, etc. (Pettijohn, 1975). Thus, it is highly likely that the most transported and well-sorted sediments like loess, fluvioeolic sand and drift sand have high quartz content which usually contains low ^{226}Ra and have low radon exhalation in the study area. In addition, the limited thickness of the hilly fluvial sediments can cause the higher soil gas radon activity concentration values in the hills, as soil gas radon activity concentration reflects more the underlying rocks.

Since the GRP spatial pattern was less variable than soil gas radon concentration, it shows the major spatial structures, whereas the soil gas radon was more sensitive to the local geological mechanisms (e.g., effects of fault lines). Fault lines are located in the mountains in the study area (Gyalog and Síkhegyi, 2010), where the higher soil gas radon activity concentration values appear. GRP involves the probability of the escape of radon from the geological formations and soils as described earlier (Eq. (1)). Permeability is spatially highly heterogeneous in the study area. The smoothing procedure on TIN maps sheds light on the fact that at larger spatial scale GRP has the same pattern as soil gas radon but at lower scale the permeability becomes dominant (Fig. 7). In addition, we made contour maps from the selected 21 × 21 window size (5250 × 5250 m) of the smoothed TIN trend surface maps and indicated the median and upper quartile in them. In both the soil gas radon concentration and GRP contour maps the upper quartiles are continuous and follow the mountainous topography well (Figs. 8 and 10), which indeed means that it corresponds to the different geologies associated to hills and mountains on the one hand, and to plains on the other hand.

This pattern cannot be related to the soil gas permeability because it does not display the same spatial pattern. In fact, soil gas permeability data have no discernable spatial pattern at all. Median and the upper-quartile contour lines in the GRP contour map provide a clearer picture of measurement trends than the usual categorization according to Neznal et al. (2004) (Fig. 10). Using the usual literature-based categorization data (Neznal et al., 2004) the GRP median (8.1) is almost the same as the low-medium GRP boundary (10), whereas the upper 25% of GRP data are much lower than the medium–high GRP boundary (35) according to the upper quartile (14.8). The reason for this is the high amount of the Quaternary sediment covering the study area, which provides low or medium geogenic radon potential for large part of the area (Fig. 4). Barnet (2008) also found, working on igneous, metamorphic and sedimentary rocks of the Czech Republic, that sedimentary rocks have mostly low soil gas radon activity concentration and radon potential in contrast to the other major rock groups.

There was a high nugget effect in the empirical variogram of the soil gas radon activity concentration and the soil gas permeability without outliers, whereas GRP had a lower nugget effect (Fig. 9) confirming the applicability of GRP.

Autocorrelation and directional variograms calculated for the smoothed TIN trend surface maps showed periodicity in the NE–SW direction (azimuth: 20° with ±15° tolerance) in soil gas radon activity concentration (Fig. 8B). Topography, ridges and also valleys in the area have an NW–SE direction, except for the N–S oriented mountains in the west, and increase of the soil gas radon activity concentration seemed to follow this topography (Fig. 8A). We checked if this is a real periodicity or induced by the dominating mountain features. Removing the mountain areas from the data along the upper quartile of the soil gas radon activity concentration contour map (Fig. 8A), the observed 27 km periodicity remained as a persistent feature (Fig. 8C). Indeed, all valleys and hills have NW–SE direction, except for the N–S oriented mountains in the west (Fig. 1). Hence, it can be concluded that soil gas radon activity concentration followed the periodically arranged topography which shows distinct directions. This clearly indicates, in turn, that the soil gas radon concentrations corresponded to the main geological, basically tectonic, structures. Influence of the fault lines on soil gas radon concentration has been already reported by Barnet (2008), Papp et al. (2010) and Swakon et al. (2005), studying granites and gneisses, andesite and carbonate rocks, respectively. All of these papers pointed out that active fault lines cause locally increasing soil gas radon activity concentration.

A two-dimensional auto-correlogram showed strong spatial autocorrelation of soil gas radon activity concentration in the N–S direction. According to the anisotropy ellipse, the anisotropy index is 0.6 (Fig. 8B). We tested the assumption that this anisotropy was due to the N–S running mountain range in the west. If the mountain areas were eliminated from the map, the N–S autocorrelation disappeared (Fig. 8B). However the strong NW–SE direction anisotropy emerges, which was also captured by the directional variograms (Fig. 8B). This confirms that the N–S anisotropy was induced by the N–S mountains and does not characterize the entire study area. The soil gas radon concentration of the whole area is characterized by a pronounced NW–SE orientation following the topography.

Auto-correlograms for soil gas permeability and for GRP show no spatial autocorrelation or anisotropy (Fig. 11). This indicates that topography had effect only on soil gas radon activity concentration and the identified anisotropy and periodicity were not related to soil gas permeability spatial distribution, but they may be related to the fault lines documented only in the mountain areas.

GRP risk map (Fig. 12) was created by attributing a GRP median value (Fig. 4) to all geological formations based on field measurements. Accordingly, mainly low and medium risk characterizes the study area. However, according to our measurements, low risk areas contained 69% low, 28% medium and 3% high GRP sites. Medium risk areas contained 29% low, 58% medium and 13% high GRP sites. This means they have a local misclassification probability

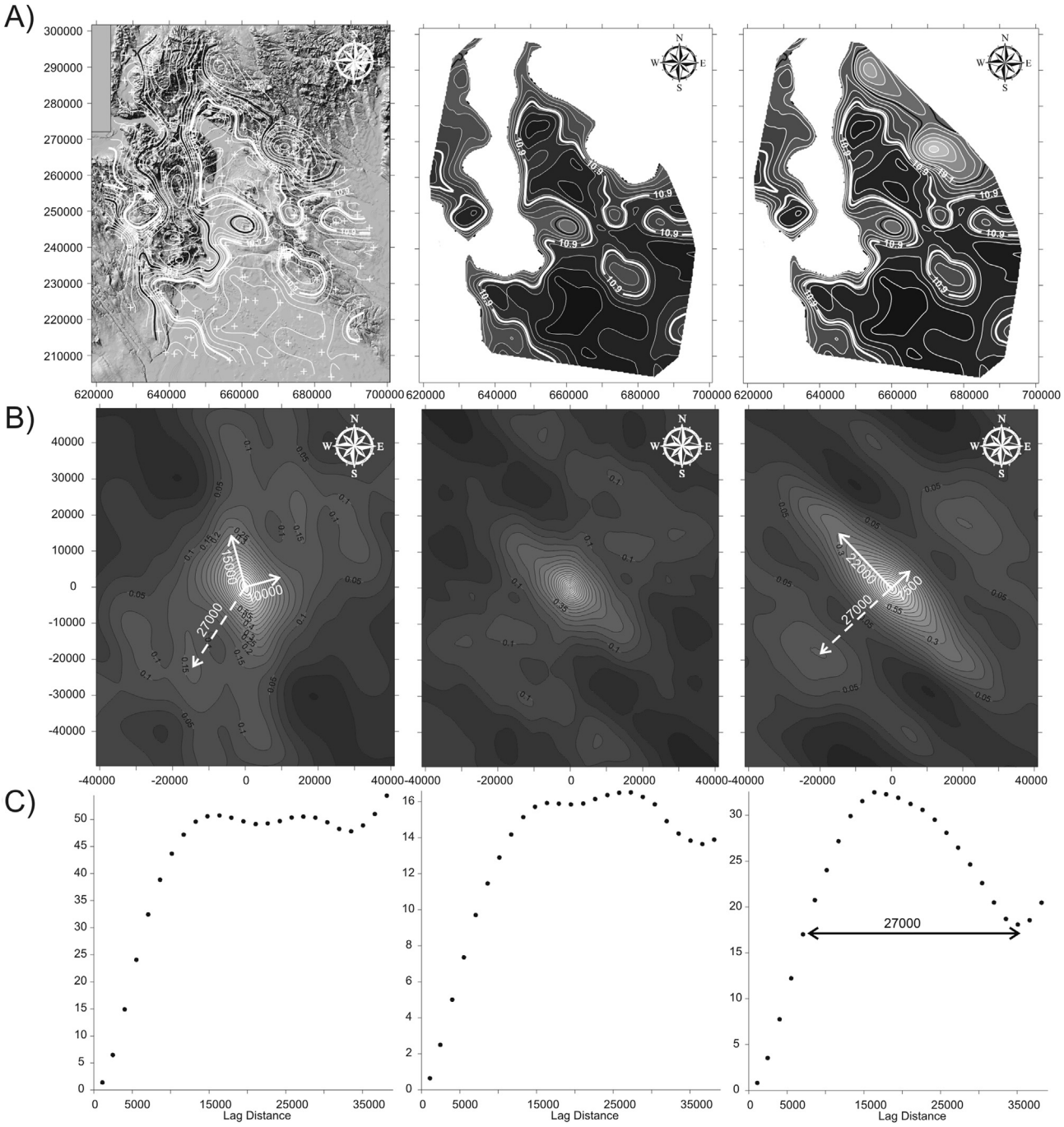

Fig. 8. A. Shaded relief map and the superimposed contour lines of the soil gas radon activity concentration (kBq m^{-3}) showing also the measurement sites (white crosses). The bold white lines indicate the median, thick black lines correspond to the upper quartile of the soil gas radon activity concentration. The map in the middle shows the contour lines of the soil gas radon activity concentration when the mountain areas removed. The map on the right shows the contour lines of the soil gas radon activity concentration when only the N–S mountain areas were removed. Mountain areas were removed along the upper quartile of the soil gas radon activity concentration (first map of this figure). B. Auto-correlograms for the soil gas radon activity concentration (kBq m^{-3}) calculated from the smoothed TIN trend surface map. White arrows indicate the direction of anisotropy, white dashed arrows correspond to periodicity of soil gas radon activity concentration. First map corresponds to all data. The middle map corresponds to data without the mountain areas (see corresponding maps in Fig. 8A), the one on the right to data when only the N–S mountains were removed. Note the strong NW–SE anisotropy and NE–SW periodicity soil gas radon activity concentration. C. Directional variograms of the maps corresponding to the soil gas radon activity concentration maps in Fig. 8A above. Variograms are in SW–NE direction (azimuth = 20°, tolerance = ±15°). Note the ca. 27 km NE–SW periodicity. Coordinates are in meters.

of 31% and 42% in case of low and medium GRP, respectively. This is the inevitable error of the classification.

Only two geological formations (fluvial–proluvial sediment, and deluvial clay and sand) had high risk. These partly affect 18 settlements in the northern part of the study area which are close to hills built-up limestone and andesite or to regions where sandstone and lignite formations dominantly occur (Fig. 12). We calculated an upper estimate of the population that lives on high risk area. It concerns approximately 0.5% of the population (15,000 persons) living in the study area. On these high risk areas detailed indoor measurements are recommended. This is supported by studies of Cosma et al. (2013), Somlai et al. (2006) and Tóth et al. (1994) who

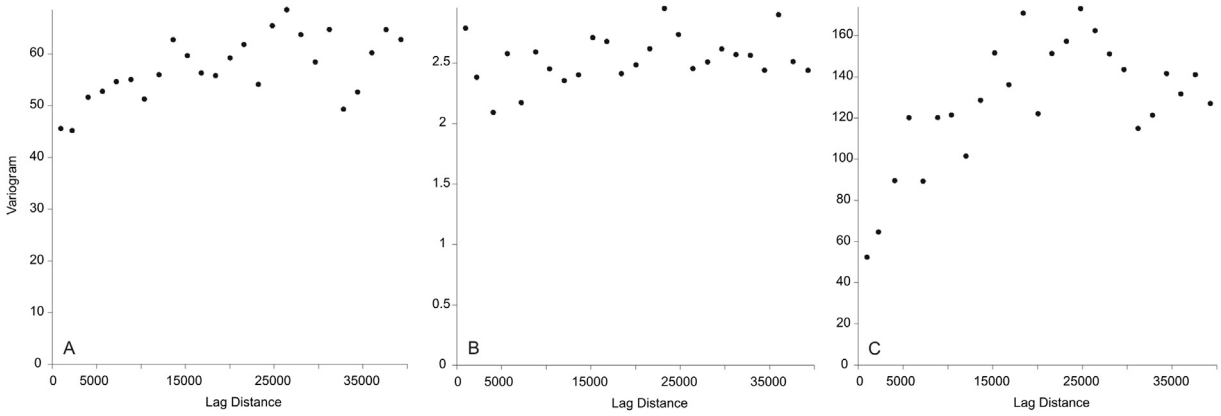

Fig. 9. Empirical variogram of the original soil gas radon activity concentration (A), soil gas permeability (B) and geogenic radon potential values (C) (without outliers).

investigated indoor radon concentration in areas of high radon potential. Cosma et al. (2013) studied indoor radon concentrations in detail at Baita-Stei, a former uranium exploitation area in NW Romania, where as high as 5000 Bq m^{-3} indoor radon concentration was found and soil radon levels ranged from 20 to 500 kBq m^{-3}. Tóth et al. (1994) and Somlai et al. (2006) also reported enhanced indoor radon concentrations (1660 Bq m^{-3} and 667 Bq m^{-3}, respectively) in the seismologically active geological overthrust zone with elevated CO_2, H_2S, CH_4 and radon exhalation at Mártaderecske (Hungary) and in area of the closed uranium mine in the Mecsek Mts. in Hungary, respectively.

Considering the five Quaternary formations, in which more than 8 samples are available, again, the fluvial sediment has medium GRP, whereas the others have low GRP. These results suggest to group together the Quaternary sediments having low GRP and low soil gas radon activity concentration (drift sand, fluvioeolic sand, fluvial sand and loess) from the radon point of view (Fig. 4).

The TIN-based contour GRP map (Fig. 10) predicts high GRP in areas where the geology-based GRP map does not (Fig. 12). The reason for this is that TIN-based contour GRP does not take into account the geology and uses smaller area for averaging compared to geology-based GRP.

However, their major patterns are the same: lower values are observed in the planes and higher values correspond to the hilly areas.

The GRP values of the 41 geological formations can be extended to the whole territory of Hungary. However, this is only a preliminary approach because the extrapolated values would have higher uncertainty than values in the studied area, which were compiled with interpolation. Since the largest part of Hungary (~75%) is covered by Quaternary sediments having low or medium geogenic radon potential, high GRP areas are expected only locally on the proluvial and deluvial sediments, rock debris on the downhill slopes eroded from hills. Also, high GRP can be predicted for the areas with granite and gneiss rocks, covering only less than approximately 5% of the Hungarian territory in the central (Velencei Mts.), western (Sopron Mts.) and southern (Mecsek Mts.) areas. Additionally, high risk area is in the vicinity of the closed uranium mine in the western part of the Mecsek Mts., where the uranium ore is located in sandstone. These predictions can be supported by several previous measurements which showed high level of indoor radon activity concentration (maximum 5.8 kBq m^{-3}) in the Mecsek Mts. at the closed uranium mine (Nagy et al., 2011) and very high radon activity concentration (maximum ~600 kBq m^{-3}) in the gneiss formation of the Sopron Mts.

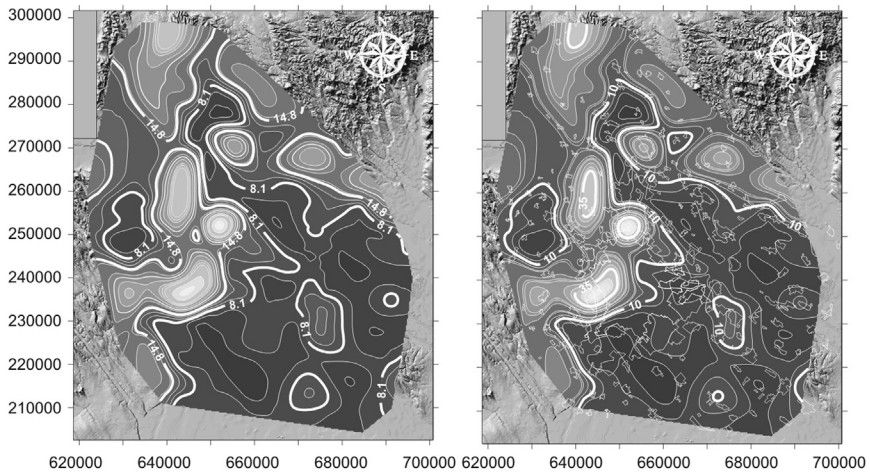

Fig. 10. Contour maps of geogenic radon potential (GRP). In the map on the left the bold white lines show the median (8.1) and the upper quartile (14.8) with the shaded relief model in the background. In the map on the right the heavy white lines correspond to the GRP categorization after Kemski et al. (2001) and shows settlements in relation to GRP levels. Note that only 5 settlements are located in the high GRP value areas.

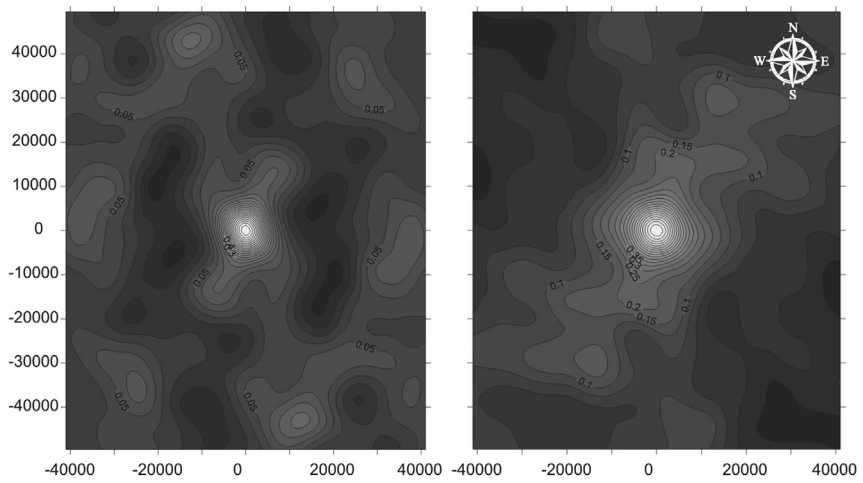

Fig. 11. Auto-correlogram of the soil gas permeability (m^2) and geogenic radon potential calculated from the smoothed TIN trend surface map. Coordinates are in meters.

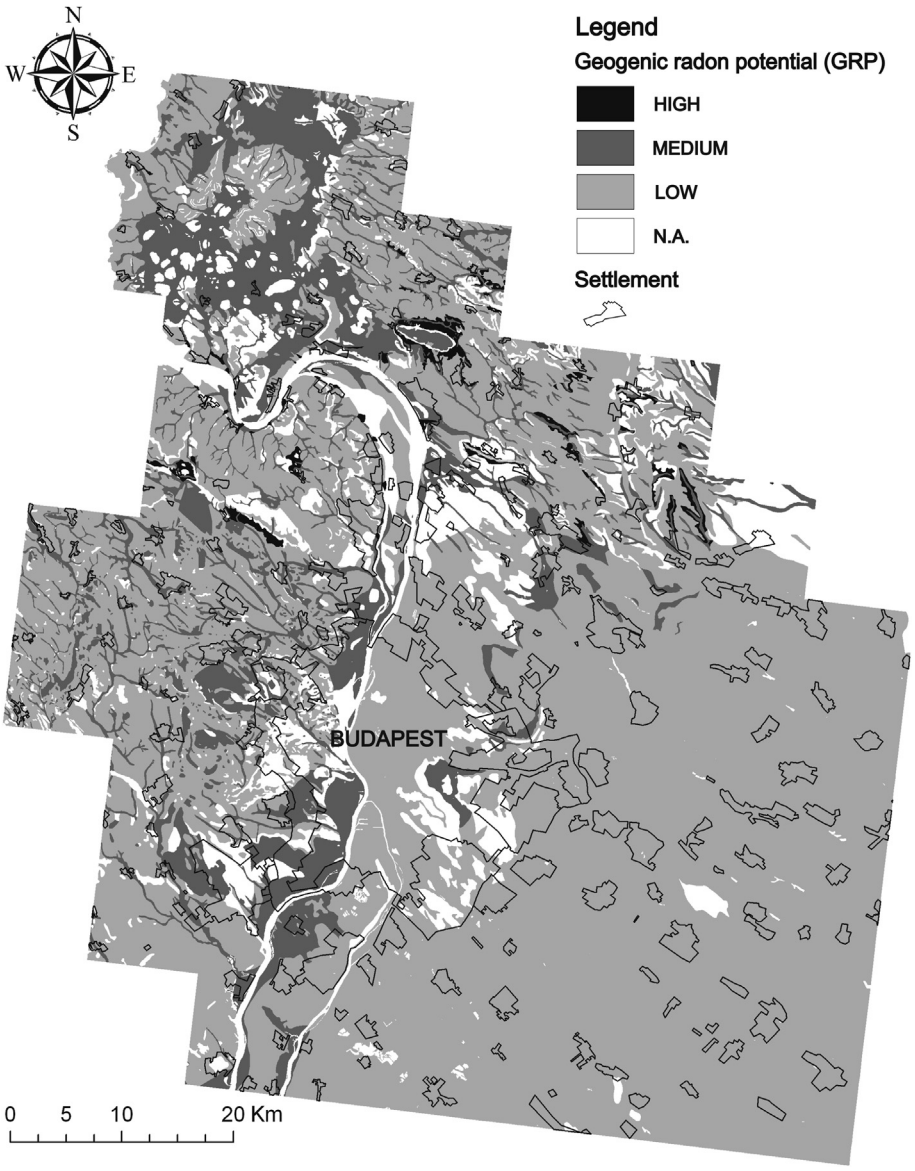

Fig. 12. GRP risk map with geogenic radon potential (GRP) values according to the geological formations in the study area. Note that 18 settlements are partly located in the high GRP value areas.

6. Concluding remarks

Geogenic radon potential mapping based on the continuous variable approach was tested in a pilot area in Hungary. As an overall result, the soil gas radon activity concentration and GRP showed a clear spatial structure confirming that the approach is correct. The first geogenic radon potential map was compiled for the central part of Hungary, which covers 6.5% of the country, and in which about 28% of the population lives. This GRP map shows that regions of low and medium geogenic radon potential characterize the study area. High risk occurs very locally only connected to proluvial and deluvial sediments of limestone and andesite mountain terrain and sandstone and lignite-bearing hilly areas and affects only the 0.5% of the population of the study area. However, there is a local misclassification probability of 31% and 42% in case of low and medium GRP, respectively.

Variable Quaternary sediments found in the study area are inhomogeneous from a radon point of view. Fluvial sediment had medium GRP, whereas the other rock formations (i.e., drift sand, fluioeolic sand, fluvial sand and loess) had low GRP. The presented GRP map will help the decision makers with radon regulation. Additionally, it may be extrapolated to the whole country with restrictions.

Exploratory data analysis revealed that soil gas permeability data had no discernable spatial pattern at the available spatial resolution of the data, whereas the soil gas radon activity concentration and GRP did have such features. The latter two had almost the same pattern, however, the GRP was less variable. Both of them follow the topography of the area. They have the same 27-km-long NE–SW periodicity as the topography represented by the digital elevation model. Moreover, a persistent NW–SE spatial anisotropy was shown in the soil gas radon activity concentration. Higher soil gas radon activity concentration and GRP characterizes the hilly areas than the plains. The highest values were found in the proluvial–deluvial sediments. These are rock debris on the downhill slopes eroded from the hills. Quaternary sediments are heterogeneous, the fluvial sediment had the highest soil gas radon activity and GRP values, which were also located on the hilly areas. The lowest values were measured in the plain areas (drift sand, fluvioeolic sand, fluvial sand and loess).

Radon is related to the erosion and deposition of the sediment cycle. Thus sediments deposited near to the sources in the mountains and hills reflect the original rock composition such as andesite, dacite and limestone and generally have medium or relatively high GRP. In contrast, sediments which are transported far and deposited on the plains as mature sediments like loess, fluvioeolic sand and drift sand have high quartz content, which usually contain low ^{226}Ra and have low radon exhalation. Thus, generally they have low GRP.

Acknowledgment

The research has been founded by the Doctoral School for Environmental Sciences, Eötvös University (Budapest) and supported by the European Union and the State of Hungary, co-financed by the European Social Fund in the framework of TÁMOP 4.2.4 A/1-11-1-2012-0001 'National Excellence Program'. This research has been carried out with the help of GEM-RG Geochemistry, Modeling and Decisions Research Group. The authors give special thank to Botond Papp and Cosma Constantin, Babes-Bolyai University, Cluj (Romania) and to Gábor Kocsy, Hungarian "Frédéric Joliot-Curie" National Research Institute for Radiobiology and Radiohygiene for the soil gas radon comparison measurement. Thanks also go to the three anonym referees and the chief- editor S.C. Sheppard for their useful comments and suggestions.

This is the 68th publication of the Lithosphere Fluid Research Laboratory (LRG) at Eötvös University.

References

Alonso, H., Rubiano, J.G., Arnedo, M.A., Gil, J.M., Rodriguez, R., Florido, R., Hartel, P., 2010. Determination of the radon potential for volcanic materials of the Gran Canaria Island. In: Barnet, I., Neznal, M., Pacherova, P. (Eds.), Proc., 10th International Workshop on the Geological Aspects of Radon Risk Mapping. Czech Geological Survey, Radon v.o.s., Prague, ISBN 978-80-7075-754-3, pp. 7–14. http://www.radon.eu/workshop2010/.

Al-Shereideh, S.A., Bataina, B.A., Ershaidat, N.M., 2006. Seasonal variations and depth dependence of soil radon concentration levels in different geological formations in Deir Abu-Said district, Irbid e Jordan. Radiat. Meas. 41, 703–707.

Appleton, J.D., Miles, J.C.H., 2010. A statistical evaluation of the geogenic controls on indoor radon concentrations and radon risk. J. Environ. Radioact. 101, 799–803.

Appleton, J.D., Miles, J.C.H., Young, M., 2011. Comparison of Northern Ireland radon maps based on indoor radon measurements and geology with maps derived by predictive modelling of airborne radiometric and ground permeability data. Sci. Tot. Environ. 409, 1572–1583.

Barbosa, S.M., Steinitz, G., Piatibratova, O., Silva, M.E., Lago, P., 2007. Radon variability at the Elat granite, Israel: heteroscedasticity and nonlinearity. Geophys. Res. Lett. 34, L15309.

Barnet, I., 1994. Radon risk classification for building purposes in the Czech Republic. In: Barnet, I., Neznal, M. (Eds.), Radon investigations in CR, vol. 5Czech Geological Survey, Prague, pp. 18–24.

Barnet, I., 2008. Radon in Geological Environment: Czech Experience. Czech Geological Survey, Prague.

Barnet, I., 2011. Indoor radon probability calculated from the Czech soil gas radon data in a grid net for the European Geogenic Radon Map construction: test of feasibility. Environ. Earth. Sci. 66, 1149–1153.

Barnet, I., Fojtíková, I., 2008. Soil gas radon, indoor radon and gamma dose rate in CZ: contribution to geostatistical methods for European Atlas of Natural Radiations. Radiat. Prot. Dosim. 130, 81–84.

Barnet, I., Mikšová, J., Fojtíková, I., 2005. Indoor – soil gas relationship in the Central Bohemian Plutonic Complex. Ann. Geophys. 48, 93–99.

Barnet, I., Pacherová, P., 2010. Generalized geological units as a background for European geogenic radon potential map – an example from the Czech Republic. In: Barnet, I., Neznal, M., Pacherova, P. (Eds.), Proc., 10th International Workshop on the Geological Aspects of Radon Risk Mapping. Czech Geological Survey, Radon v.o.s., Prague, ISBN 978-80-7075-754-3, pp. 35–41. http://www.radon.eu/workshop2010/.

Baykut, S., Akgül, T., Inan, S., Seyis, C., 2010. Observation and removal of daily quasi-periodic components in soil radon data. Radiat. Meas. 45, 872–879.

Bertolo, A., Verdi, L., 2001. Validation of a geographic information system for the evaluation of the soil radon exhalation potential in South-Tyrol and Veneto (Italy). Radiat. Prot. Dosim. 97, 321–324.

Bossew, P., Dubios, G., Tollefsen, T., 2008. Investigations on indoor Radon in Austria, part 2: geological classes as categorical external drift for spatial modeling of the Radon potential. J. Environ. Radioact. 99, 81–97.

Chen, J., 2009. A preliminary design of a radon potential map for Canada: a multi-tier approach. Environ. Earth Sci. 59, 775–782.

Chen, J., Falcomer, R., Bergman, L., Wierdsma, J., Ly, J., 2009. Correlation of soil radon and permeability with indoor radon potential in Ottawa. Radiat. Prot. Dosim. 136, 56–60.

Chen, J., Moir, D., MacLellan, K., Leigh, E., Nunez, D., Murphy, S., Ford, K., 2012. Preliminary findings of radon potential indexes in five Canadian cities. Environ. Nat. Resour. Res. 2, 2–9.

Cosma, C., Cucoş-Dinu, A., Papp, B., Begy, R., Sainz, C., 2013. Soil and building material as main sources of indoor radon in Băiţa-Ştei radon prone area (Romania). J. Environ. Radioact. 116, 174–179.

Crockett, R.G.M., Perrier, F., Richon, P., 2010. Spectral-decomposition techniques for the identification of periodic and anomalous phenomena in radon time-series. Nat. Hazards Earth Syst. Sci. 10, 559–564.

Damkjaer, A., Korsbech, U., 1992. A small-diameter probe for in situ measurements of gas permeability of soils. Radiat. Prot. Dosim. 45, 85–89.

De Cort, M. (Ed.), 2010. Advances in Radon Mapping. J. Environ. Radioact. 101, 785–894.

Dehandschutter, B., Ciotolli, G., 2010. Detailed-scale radon hazard mapping combining indoor, soil gas and geological data. In: Barnet, I., Neznal, M., Pacherova, P. (Eds.), Proc., 10th International Workshop on the Geological Aspects of Radon Risk Mapping. Czech Geological Survey, Radon v.o.s., Prague, ISBN 978-80-7075-754-3, pp. 92–99. http://www.radon.eu/workshop2010/.

Dubois, G., Bossew, P., Tollefsen, T., De Cort, M., 2010. First steps towards a European atlas of natural radiation: status of the European indoor radon map. J. Environ. Radioact. 101, 786–798.

Dubois, G.A.G., 2005. An Overview of Radon Surveys in Europe. European Communities, Luxembourg.

Durridge Company Inc.., 2000. RAD7 Electronic Radon Detector, User Manual.

Friedmann, H., 2005. Final results of the Austrian radon project. Health Phys. 89, 339–348.

Guibas, L., Stolfi, J., 1985. Primitives for the manipulation of general subdivisions and the computation of Voronoi diagrams. ACM Trans. Graph. 4, 74–123.

Guida, D., Guida, M., Cuomo, A., Guadagnuolo, D., Siervo, V., 2010. Radon-prone area assessment by means of multi-scale hierarchical approach. Case study of the

Campania region, Southern Italy. In: Barnet, I., Neznal, M., Pacherova, P. (Eds.), Proc., 10th International Workshop on the Geological Aspects of Radon Risk Mapping. Czech Geological Survey, Radon v.o.s., Prague, ISBN 978-80-7075-754-3, pp. 122–139. http://www.radon.eu/workshop2010/.

Gyalog, L. (Ed.), 1996. Signal Code of the Geological Maps and Short Description of the Stratigraphical Units I (In Hungarian). Geological Institute of Hungary, Budapest. Special Paper 187.

Gyalog, L., Síkhegyi, F. (Eds.), 2010. 1:100.000 Geological Map of Hungary. Geological Institute of Hungary, Budapest (CD-ROM).

Hámori, K., Tóth, E., Losonci, A., Minda, M., 2006a. Some remarks on the indoor radon distribution in a country. Appl. Radiat. Isot. 64, 859–863.

Hámori, K., Tóth, E., Pál, L., Köteles, Gy., Losonci, A., Minda, M., 2006b. Evaluation of indoor radon measurements, in Hungary. J. Environ. Radioact. 88, 189–198.

Ielsch, G., Cushing, M.E., Combes, Ph., Cuney, M., 2010. Mapping of the geogenic radon potential in France to improve radon risk management: methodology and first applications to region Bourgogne. J. Environ. Radioact. 101, 813–820.

Kemski, J., Klingel, R., Siehl, A., Stegemann, R., 2005. Radon transfer from ground to houses and prediction of indoor radon in Germany based on geological information. Radioact. Environ. 7, 820–832.

Kemski, J., Siehl, A., Stegemann, R., Valdivia-Manchego, M., 2001. Mapping the geogenic radon potential in Germany. Sci. Tot. Environ. 272, 217–230.

Kolmogorov, A., 1933. Sulla determinazione empirica di una legge di distribuzione. G. Inst. Ital. Attuari 4, 83.

Koorevaar, P., Menelik, G., Dirksen, C., 1983. Elements of Soil Physics. In: Developments in Soil Science, vol. 13. Elsevier, Amsterdam, New York.

Kruskal, W.H., Wallis, W.A., 1952. Use of ranks in one-criterion variance analysis. J. Am. Stat. Assoc. 47, 583–621.

Kumar, A.V., Sitaraman, V., Oza, R.B., Krishnamoorthy, T.M., 1999. Application of a numerical model for the planetary boundary layer to the vertical distribution of radon and its daughter products. Atmos. Environ. 33, 4717–4726.

Levene, H., 1960. Robust tests for equality of variances. In: Olkin, I., Hotelling, H., et al. (Eds.), Contributions to Probability and Statistics: Essays in Honor of Harold Hotelling. Stanford University Press, pp. 278–292.

Mann, H.B., Whitney, D.R., 1947. On a test of whether one of two random variables is stochastically larger than the other. Ann. Math. Stat. 18, 50–60.

Miles, J.H.C., Appleton, J.D., 2005. Mapping variation in radon potential both between and within geological units. J. Radiol. Prot. 25, 257–276.

Miles, J.H.C., Green, B.M.R., Lomas, P.R., Cliff, K.D., 1991. Radon in UK homes: defining the areas affected. Radiat. Prot. Dosim. 36, 117–120.

Minda, M., Tóth, Gy., Horváth, I., Barnet, I., Hámori, K., Tóth, E., 2009. Indoor radon mapping and its relation to geology in Hungary. Environ. Geol. 57, 601–609.

Nagy, H.E., Breitner, D., Horváth, Á., Szabó, C., 2011. Study of a passive radon mingation process and indorr radon concentration's time dependence after mitigation. Carpath. J. Earth Environ. Sci. 6, 143–149.

Neznal, M., Neznal, M., 2006. Reliability of the new method for assessing the radon risk – gas permeability classification. In: Barnet, I., Neznal, M., Pacherová, P. (Eds.), Radon Investigations in the Czech Republic XI and the 8th International Workshop on the Geological Aspects of Radon Risk Mapping. Czech Geological Survey/Radon v.o.s./JRC-IES-REM, Ispra, Prague, pp. 166–172.

Neznal, M., Neznal, M., Matolin, M., Barnet, I., Miksova, J., 2004. The New Method for Assessing the Radon Risk of Building Sites. In: Czech Geol. Survey Special Papers, vol. 16. Czech Geol. Survey, Prague. http://www.radon-vos.cz/pdf/metodika.pdf.

Neznal, M., Neznal, M., Šmarda, J., 1995. Temporal variability of soil gas radon concentration – some remarks. In: Dubois, C. (Ed.), Gas Geochemistry. Science Reviews, Northwood, pp. 529–534.

Neznal, M., Pernička, F., 1996. Temporal changes of soil-gas radon concentration at a test site – uranium mill tailings. In: Barnet, I. (Ed.), Radon investigations in the Czech Republic, vol. 6Czech Geological Survey, Prague, pp. 79–87.

OMSZ (Hungarian Meteorological Service). Climate of Hungary (online database), www.met.hu/eghajlat/magyarorszag_eghajlata.

Papp, B., Szakács, A., Néda, T., Papp, S., Cosma, C., 2010. Soil radon and thoron studies near the mofettes at Harghita Bai (Romania) and their relation to the field location of fault zones. Geofluids 10, 586–593.

Perrier, F., Richon, P., Sabroux, J.C., 2009. Temporal variations of radon concentration in the saturated soil of Alpine grassland: the role of groundwater flow. Sci. Tot. Environ. 407, 2361–2371.

Pettijohn, F.J., 1975. Sedimentary Rocks, third ed. Addison-Wesley, New York.

Reimann, C., Filzmoser, P., Garrett, R.G., Dutter, R., 2008. Statistical Data Analysis Explained. Applied Environmental Statistics with R. Wiley, Chichester.

Rodgers, J.L., Nicewander, W.A., 1988. Thirteen ways to look at the correlation coefficient. Am. Stat. 42, 59–66.

Schumann, R.R., 1993. Geologic radon potential of the glaciated Upper Midwest. In: Proceedings: The 1992 International Symposium on Radon and Radon Reduction Technology. Symposium Oral Papers, Technical Sessions VII–XII, vol. 2. U.S. Environmental Protection Agency Rept. EPA-600/R-93/083b, Research Triangle Park, N.C., 8–33–8–49. www version: http://energy.cr.usgs.gov/radon/midwest1.html (accessed 28.07.13).

Smetanová, I., Holy, K., Müllerová, M., Poláskova, A., 2010. The effect of meteorological parameters on radon concentration in borehole air and water. J. Radioanal. Nucl. Chem. 283, 101–109.

Smirnov, N.V., 1948. Tables for estimating the goodness of fit of empirical distributions. Ann. Math. Stat. 19, 279–281.

Somlai, J., Gorjánácz, Z., Várhegyi, A., Kovács, T., 2006. Radon concentration in houses over a closed Hungarian uranium mine. Sci. Tot. Environ. 367, 653–665.

Sundal, A.V., Valen, V., Soldal, O., Strand, T., 2008. The influence of meteorological parameters on soil radon levels in permeable glacial sediments. Sci. Tot. Environ. 389, 418–428.

Swakon, J., Kozak, K., Paszkowski, M., Gradzinski, R., Loskiewicz, J., Mazur, J., Janik, M., Bogacz, J., Horwacik, T., Olko, P., 2005. Radon concentration in soil gas around local disjunctive tectonic zones in the Krakow area. J. Environ. Radioact. 78, 137–149.

Szabó, K.Z., Jordan, G., Horváth, Á., Szabó, C., 2013. Dynamics of soil gas radon concentration in a highly permeable soil based on a long-term high temporal resolution observation series. J. Environ. Radioact. 214, 74–83.

Tollefsen, T., Gruber, V., Bossew, P., De Cort, M., 2011. Status of the European indoor radon map. Radiat. Prot. Dosim. 145, 110–116.

Tóth, E., Boros, D., Samuelsson, L., Deák, F., Marx, G., Sükösd, C., 1994. High radon activity in northeast. Hung. Phys. Scr. 50, 726–730.

Tóth, E., Hámori, K., Minda, M., 2006. Indoor radon in Hungary (lognormal mysticism). In: Barnet, I., Neznal, M., Pacherová, P. (Eds.), Radon Investigations in the Czech Republic XI and the 8th International Workshop on the Geological Aspects of Radon Risk Mapping. Czech Geological Survey/Radon v.o.s./JRC-IES-REM, Ispra, Prague, pp. 252–257,.

Tukey, J.W., 1977. Exploratory Data Analysis. Addison-Wesley.

UNSCEAR, 2000. Sources and Effects of Ionizing Radiation. In: Effects, Annex B, vol. II. United Nations, New York.

van der Graaf, E.R., de Meijer, R.J., 1992. Calculation of Shape Factors and Pressure Fields Around an Ellipsoidal Permeability Probe in Some Simple Geometries. Tech. Doc. KVI/RV-06. Kernfysisch Versneller Instituut, Groningen, The Netherlands.

WHO, 2009. WHO Handbook on Indoor Radon – a Public Health Perspective. www.who.int/ionizing_radiation/env/radon/en/index1.html.

Winkler, R., Ruckerbauer, F., Bunzl, K., 2001. Radon concentration in soil gas: a comparison of the variability resulting from different methods, spatial heterogeneity and seasonal fluctuations. Sci. Tot. Environ. 272, 273–282.